Spatiotemporal Visualization of Subcellular Dynamics of Carbon Nanotubes

Maged F. Serag,[1] Kevin Braeckmans,[2,3] Satoshi Habuchi,[1] Noritada Kaji,[4] Alberto Bianco[5] and Yoshinobu Baba[4,6]*

[1] Chemical and Life Sciences and Engineering Division, King Abdullah University of Science and Technology, Thuwal 23955-6900, SAUDI ARABIA. [2] Biophotonic Imaging Group, Laboratory of General Biochemistry and Physical Pharmacy, Ghent University, Harelbekestraat 72, B-9000 Gent, BELGIUM. [3] Centre for Nano- and Biophotonics, Ghent University, Harelbekestraat 72, B-9000 Gent, Belgium. [4] FIRST Research Center for Innovative Nanodevices, Nagoya University, JAPAN. [5] Centre National de la Recherche Scientifique, Institut de Biologie Moléculaire et Cellulaire, UPR 9021 Immunologie et Chimie Thérapeutiques, Strasbourg, FRANCE. [6] National Institute of Advanced Industrial Science and Technology (AIST), Takamatsu, JAPAN. * Address correspondence to: magedserag@yahoo.com

KEYWORDS: carbon nanotubes, raster scan image correlation spectroscopy, plant cell, transport, diffusion, autophagy.

ABSTRACT

To date, there is no consensus on the relationship between the physicochemical characteristics of carbon nanotubes (CNTs) and their biological behavior, however, there is growing evidence that the versatile characteristics make their biological fate largely unpredictable and remain an issue of limited knowledge. Here we introduce an experimental methodology for tracking and visualization of post-uptake behavior and the intracellular fate of CNTs based on the spatial distribution of diffusion values throughout the plant cell. By using raster scan image correlation spectroscopy (RICS), we were able to generate highly quantitative spatial maps of CNTs diffusion in different cell compartments. The spatial map of diffusion values revealed that the uptake of CNTs is associated with important subcellular events such as carrier-mediated vacuolar transport and autophagy. These results show that RICS is a useful methodology to elucidate the intracellular behavior mechanisms of carbon nanotubes and potentially other fluorescently labeled nanoparticles, which is of relevance for the important issues related to the environmental impact and health hazards.

Over the past years, considerable efforts have been devoted to study the impact and effect of CNTs in living cells and to investigate their cellular fate after internalization.[1-8] These efforts were motivated by the fact that the subcellular behavior of CNTs is a critical issue that will help to evaluate the health and environmental impacts and to determine any future biological application of these nanomaterials. Perhaps the most commonly used technology to study the post-uptake behavior of CNTs is by fluorescence microscopy.[1-12] However, the insight provided by these studies did not tell much about the spatiotemporal behavior of CNTs which is needed to track and understand their intracellular behavior and fate.[10-12] Therefore, experimental tools that allow facile study of the spatiotemporal interactions between CNTs and subcellular components for visualization and tracking of post-uptake behavior are needed.

In order to visualize the spatiotemporal behavior of SWNTs, we have evaluated raster scan image correlation spectroscopy (RICS) to track the subcellular dynamic behavior associated with single walled carbon nanotubes (SWNTs) diffusion and transport (see Supporting Text I for details on this technique). RICS is intriguing for the measurement of molecular diffusion, transport and biomolecular interactions because of its single molecule sensitivity.[13] The large bandwidth, compatibility with well-established microscopy techniques and the availability of powerful data analysis platforms have made it the method of choice to study transport problems in cells and molecular aggregation.[14] RICS is a noninvasive image analysis technique based on fluorescence fluctuation correlation analysis. RICS can detect and quantify dynamic events in live cells. Molecular dynamics on time scales ranging from microseconds to milliseconds can be measured by RICS.[15-17] The basic idea behind the RICS approach is that the molecular dynamics cause fluctuations in fluorescence intensity at a given pixel during confocal imaging. Upon movement of the molecules to a neighboring pixel, the fluorescence fluctuations propagate to the new pixel and can be correlated with that of the original pixel with a certain time delay.[18] This

spatial correlation during the raster confocal scanning occurs in a scale that depends on the diffusion rate of the fluorescent molecules controlled by viscosity of the medium and/or binding/unbinding dynamics. Therefore, the analysis of the RICS signals helps to extract information about two important processes in cells, consisting of diffusion and binding/unbinding of fluorescent molecules to specific locations in the cells.[16]

Previous studies on the subcellular distribution of SWNTs showed that attaching fluorescein isothiocyanate (FITC) to their walls rendered their cellular fate controllable.[6,8,10,11] FITC molecules have the ability to cross the cell wall and the cell membrane of the plant cell. Once inside the cell, they become negatively charged in the slightly alkaline cytoplasmic compartment (SI Fig. S1). The negatively charged molecules are rapidly cleared into the acidic vacuole *via* organic anion transporters distributed through the vacuolar membrane (tonoplast). Blocking this pathway *via* probenecid, a uricosuric drug capable of inhibiting the carrier-mediated transport through the tonoplast, causes the molecules to exclusively accumulate in the cytoplasm. The removal of probenecid from the incubation medium results in exclusive re-accumulation of FITC inside the cell vacuole. It was found that SWCNT with stacked FITC follow the same pathway of cytoplasmic/vacuolar re-accumulation as free FITC. Once inside the vacuole, SWCNTs with stacked FITC are exocytosed *via* vesicle mediated transport where large exocytosis vesicles shuttle between the vacuolar and cell membranes to expel SWCNTs out of the cell (SI Fig. S1).[10] Therefore, we utilized the basic knowledge provided by these studies to direct SWNTs to either the cytoplasm or the cell vacuole and to study their spatiotemporal behavior throughout the cell *via* RICS.

The first step in any RICS measurement by confocal microscopy is to calibrate the focal volume of the laser beam waist by fitting the RICS function of a fluorophore of known diffusion coefficient (D). Rhodamine-6G ($D = 426\ \mu m^2\ s^{-1}$ at 25°C)[19] was used for daily calibration of the

focal volume prior to RICS measurements. Furthermore, the laser transmission was optimized to provide a reasonable ratio between the magnitude of the correlation fit at origin [$G_{RICS}(0)$] and the residuals-of-the-fit (R_f).[15] The $G_{RICS}(0)/R_f$ ratio of 8:1 was chosen to calculate the laser beam waist. Higher laser transmission–though providing higher $G_{RICS}(0)/R_f$ ratios–were excluded to avoid photobleaching (Table a in Fig. 1, SI Fig. S2). Since FITC was found to be a suitable functional tag to direct SWNTs toward specific cellular compartments,[10] we employed FITC as fluorescent probe and as a cellular-address tag to guide SWNTs to the cell vacuole and/or to the cytoplasm. Initially, free FITC in PBS was used as a control to optimize the imaging conditions. This control measurement was necessary[15] to achieve a reasonable $G_{RICS}(0)/R_f$ ratio at a reduced laser transmission to avoid the fast rate of photobleaching of FITC.[20] Laser transmission as low as 0.5% was found to be reliable in fitting the correlation function while providing a diffusion coefficient value ($D = 272\pm30$ $\mu m^2 s^{-1}$ at 25°C in PBS) in close agreement with the standard diffusion value of FITC ($D = 270$ $\mu m^2 s^{-1}$)[21] under the same conditions (Fig. 1b). SWNTs were ultra-shortened and functionalized by ultrasonic-assisted chemical oxidative cutting and then fluorescently labeled with fluorescein via π-stacking (hereafter referred as F-SWNTs). RICS analysis of F-SWNTs resulted in a diffusion rate of 90 ± 8 $\mu m^2 s^{-1}$ in PBS under the same conditions (Fig. 1c).

To investigate the dynamic behavior of FITC inside living cells, we used suspended cells of the genetically recalcitrant plant model *Catharanthus roseus*.[22] Following incubation with free unbound FITC, the fluorescence signals were localized in both the cytoplasm and the cell vacuoles (Fig. 2a). RICS analysis of the FITC vacuolar diffusion resulted in a diffusion value of 132 ± 9 $\mu m^2 s^{-1}$ (Fig. 2a, SI Fig. S3). This diffusion value was in a close approximate to our reported range (120-150 $\mu m^2 s^{-1}$) of FITC diffusion in the vacuoles of *Catharanthus* cells.[10] A small area of the cell was, then, selected with the zoom tool (white box in Figure 2b) and 50

frames were collected (the average intensity is shown in Figure 2b, which includes part of the vacuole and cytoplasm). Subsequently, RICS was applied to the ROI shown in Figure 2b. Based on RICS measurements, the average diffusion value of FITC in cytoplasm of *Catharanthus* cells was 1.8±0.2 $\mu m^2 s^{-1}$ (Fig. 2c,d).

Our primary objective in this study was to spatially resolve the transport and diffusion behaviors of F-SWNTs inside cells to identify the associated subcellular events. Because SWNTs with stacked FITC molecules penetrate into the vacuoles through the tonoplast *via* protein carriers, it was expected that the mobility and distribution of F-SWNTs in the cytoplasm and through the tonoplast would be complex compared to unbound FITC. RICS analysis of cells pre-incubated with F-SWNTs is shown in Figure 3a. The average diffusion of F-SWNTS in the cell vacuole was 61± 20 and ~ 0.99 $\mu m^2 s^{-1}$ in the cytoplasm. Since this is two orders of magnitude less than that of free unbound FITC, this indicated an increase in the molecular size of the diffusing species. To dissect the transport and diffusion behavior of FITC and F-SWNTs, we performed the analysis in three consecutive steps. First, spatial diffusion maps of the whole images shown in Figures 2b and 3a were constructed by sequentially selecting a 64 × 64 pixel box spaced by 32 pixel steps (Figs. 3b,d).[15] Each box was correlated and fitted independently. Then, the fit parameters–appearing to be outliers–were eliminated by changing their value in the fit map to zero (Figs. 3b, d, see Supporting Text II). Second, to track the temporal change in the spatial heterogeneity of diffusion we proposed to perform RICS analysis on two raster scan images with ~ 20 s delay (Fig. 3b). Third, to obtain the precise values at the tonoplast, we eliminated the faster values existing in the cytoplasm so as to resolve the molecular transport in the tonoplast (Figs. 3c,e).

From the diffusion maps shown in Figs. 3b-e, we observed that FITC diffuses faster than F-SWNTs in cytoplasm and at both the plasmalemma and the tonoplast (Fig. 3c,e). With the aid of

spatial scan analysis (see the experimental section below), it was observed that the FITC diffusion in cytoplasm can slow down to values of ~ 0.24 $\mu m^2 s^{-1}$ (Fig. 3c), while F-SWNTs diffusion can slow down to values of ~ 0.1 $\mu m^2 s^{-1}$ (Fig. 3e). This difference in diffusion values across the cell further proved that FITC molecules are most likely moving as stacked complexes with SWNTs. Interestingly, *Catharanthus* cells incubated in free FITC showed large spatial heterogeneity–in terms of FITC diffusion–from 0.24 up to 3.99 $\mu m^2 s^{-1}$ (see the spatial heterogeneity quantitative maps in Supplementary text II). This large heterogeneity suggested the presence of cytoplasmic micrometer-size domains, in which the dynamics of FITC are largely affected by its binding[23] to various subcellular proteins. Nevertheless, *Catharanthus* cells incubated in F-SWNTs exhibited much less spatial heterogeneity compared to FITC (from 0.1 up to 0.77 $\mu m^2 s^{-1}$; see the spatial heterogeneity quantitative maps in Supplementary Text II). Since the FITC-protein binding ability appeared not to have a significant impact on the distribution of the diffusion values of F-SWNTs in the cytoplasm, we concluded and further supported our previous finding[10] that the stacking of FITC onto the surface of SWNTs reduces its protein-binding capabilities. This observation indeed demonstrates that the quantitative spatial heterogeneity maps–as calculated *via* RICS measurements–could help to characterize the binding behavior of labeled nanotubes inside the cells.

The faster subcellular diffusion of FITC enabled temporal visualization of changes in their spatial heterogeneity within 20 s (Fig. 3b). These changes are possibly governed by the distribution of subcellular organelles. This indeed offered a close-up temporal view of FITC behavior inside *Catharanthus* cells. Nevertheless, we found that the slower diffusion of F-SWNTs was less likely to be tracked in the cytoplasm (Fig. 3d). This is possibly because that the sensitivity of the RICS approach is limited to diffusion values between (0.1 – 1,000 $\mu m^2 s^{-1}$)[15] and, therefore, the slow cytoplasmic diffusion of F-SWNTs was around the lower limit of RICS

detection. Although the temporal tracking of the spatial heterogeneity of diffusion was not successful for F-SWNTs, the successful temporal tracking of FITC diffusion exploits a powerful feature of the RICS analysis. This feature can be applied to investigate the temporal change in molecular dynamics of other nanomaterials with faster subcellular diffusion.

By scaling-up the molecular transport at the tonoplast barrier, the carrier-mediated molecular transport of FITC was resolved and showed an uninterrupted distribution through the tonoplast (Fig. 3c and Supplementary Text II). Because the transport of FITC through the tonoplast occurs exclusively *via* protein carriers,[10] this observation suggested that the protein carriers are continuously distributed–or at least within the resolution of the measurements–through the tonoplast. Surprisingly, and in contrast to FITC, the transport of F-SWNTS through the tonoplast appeared interrupted at defined zones (Fig. 3e and Supplementary Text II). In an attempt to further resolve this behavior, we analyzed the raster scan images with a smaller region of interest (32 × 32 pixels) that was systematically moved across the images by steps of 16 pixels to increase the resolution of the spatial maps. Interestingly, the cytoplasmic spatial diffusion of F-SWCNTs toward the cell vacuole appeared continuous in the cytoplasm and extends into the vacuole through defined zones of the tonoplast. Moreover, we found that zones of the tonoplast, which are very near to the shuttling exocytosis, are not marked with transport activity (SI Fig. S4). This could explain the zoned vacuolar transport behavior at the tonoplast where the vesicle budding/fusion with tonoplast[10] at defined zones might interrupt the carrier-mediated vacuolar uptake of F-SWCNTs (SI Fig. S4).

The diffusion values of F-SWNTs accumulating at the vacuolar side of the tonoplast of some cells (SI Fig. S4a) did not show up the recorded fast diffusion values of 60± 20 $\mu m^2 s^{-1}$. Rather, it indicated similar values to the cytoplasmic diffusion of F-SWNTs (Fig. 3d). To further explore this observation, we incubated *Catharanthus* cells with F-SWNTs in medium containing

probenecid to inhibit the carrier-mediated transport of F-SWCNTs. Following the incubation with probenecid and RICS analysis, the molecular transport at the tonoplast was accordingly inhibited with no evidence of vacuolar accumulation of F-SWCNTs (Figs. 4a-c, SI Fig. S5a). Interestingly, we were able, however, to identify a slow and localized form of diffusion spreading into the vacuole through the tonoplast of some cells (Figs. 4a-c, SI Figs. S5b-e). The diffusion values of F-SWNTs in cell vacuoles resulting from this form of diffusion were still comparable to the cytoplasmic diffusion values of F-SWNTs (Figs. 3e, 4c). This indicated that a part of the cytoplasmic material, associated with F-SWNTs, is penetrating into the vacuole. This unique spatial distribution of diffusion values in comparison with the control values lead us to hypothesize that the occurrence of autophagy ('self-eating') as an important post-uptake behavior induced by the SWNTs. It is essential to note that autophagy is an ubiquitous stress response in eukaryotic organisms that targets damaged organelles for vacuolar degradation.[24] Therefore, autophagy can be understood as a protective cellular response that help the cell to eliminate SWNTs with the damaged organelles into the lytic vacuole. Autophagy could represent a protective mechanism working together with the vesicle mediated transport to eliminate SWCNTs accumulating inside the vacuole.

To further support this mechanism of organelles recycling and SWNTS vacuolar clearance, we decided to investigate the tonoplast ultrastructure using high resolution transmission electron microscopy (HRTEM). Interestingly, HRTEM image of *Catharanthus* cells incubated with F-SWNTs showed the autophagy response at the tonoplast (Fig. 4d,e). Autophagy in F-SWNTs-incubated cells was evidenced through the appearance of damaged Golgi bodies (Fig. 4d, SI Fig. S6) in cell vacuoles while no sign of autophagy was observed in control cells incubated in F-SWNTs-free medium (Fig. 4f). Taken together, RICS and HRTEM analyses suggested that F-SWNTS could enter cell vacuoles through autophagy as a response of SWNTs-induced stress

which we propose to cause damage to some organelles. These results documented the first spatiotemporal mapping of CNTs behavior inside living cells and provided a functional platform to visualize and study vital cellular processes such as carrier-mediated transport and autophagy.

In summary, the data resulted from this study aimed at introducing a new experimental methodology to act in concert with a technically very important nanomaterial to visualize and track poorly understood subcellular events. We proposed to harness the unique spatiotemporal performance of RICS analyses with the unique physicochemical characteristics of CNTs to induce, track and understand specific cellular responses. In our study, the subcellular dynamics of CNTs, revealed *via* RICS and supported with HRTEM analysis, provided clear evidence of CNT-associated carrier-mediated transport and CNT-induced autophagy. Depending on the application, it would be interesting to have CNTs affecting the cellular behavior in a specific manner. While endogenous autophagy could be passively-labeled with specific dyes, our study was able to demonstrate CNTs as a new class of autophagy inducers. These active-labels of autophagy would open new opportunities to understand a broad range of associated cellular responses. Although extensive knowledge of autophagy and membrane trafficking mechanisms in yeast and mammals has been achieved, understanding and direct experimental molecular data on plant autophagy still remain rather limited.[24] Furthermore, if exploited in mammalian cells, inducing autophagy could be a therapeutic target for some diseases.[25] Therefore, our experimental methodology and tools with built-in capabilities for *in vivo* tracking, spatial resolution, quantitative spatial heterogeneity and targeting specific cellular responses are expected to open a new route for a multitude of diverse biotechnological applications of targeting and understanding subcellular processes. This would bring about valuable advances in subcellular nanobiology and could be used for the assessment of environmental and health impacts of nanomaterials.

Experimental section

Carbon nanotubes: Carboxylic acid functionalized single walled carbon nanotubes (SWNTs) were purchased from Sigma-Aldrich (St. Louis, MO, USA). The bundle dimensions were D × L: 4-5 nm × 0.5-1.5 μm. SWNTs were shortened *via* sonication and acid treatment as described elsewhere.[10] FITC-labeled SWNTs (F-SWNTs) were prepared by mixing under sonication 1 mL of oxidized SWNTs (200 μg/mL) and 10 μL of 1 mg/mL FITC (Invitrogen, Carlsbad, CA, USA) for 10 min at 0 °C, followed by centrifugation to remove impurities. The solution was then transferred to a dialysis film (FED, Rancho Dominguez, CA, USA; MWCO 3.5-5 KD) to remove free FITC.

Plant Material: *Catharanthus roseus* cell suspension culture originating from callus culture was initiated in Murashig and Skoog medium (pH=5.8) with minimal organics (MSMO, Sigma, St. Louis, MO, USA) supplemented with 1 μM 2,4-dichlorophenoxyacetic acid and 1 μM kinetin. The culture and incubation procedures with FITC and F-SWNTs were essentially the same as described previously.[10] To study the effect of probenecid, 5 mM probenecid was added to the cell suspension followed by 100 μL of F-SWNTs solution to achieve a concentration of 5 μg/mL.

Confocal microscopy imaging of living cells: After incubation with FITC, cells were stored at 4° C and imaged directly to avoid the fast clearance of the FITC into the vacuoles via the protein transporters. Three hundred μL of cell suspension was placed in glass bottom dishes (Matsunami, Kishiwada, Osaka, Japan). Live cell images were taken using 10×, 40× and 100× objectives lenses on both a laser scanning confocal microscope (Olympus, FV1000). The Olympus microscope was equipped with a multi-line Ar laser (458 nm, 488 nm, 515 nm), a HeNe(G) laser (543 nm, 1 mW), and an AOTF laser combiner plus a set of ion deposition and barrier filters. Images were acquired and analyzed using Fluoview software.

Raster scan image correlation spectroscopy: Olympus FV 1000 microscope with 60× 1.25NA oil objective (Olympus, Tokyo, Japan). The scan speed was set at 8 μs/pixel (Rhodamine-6G and FITC controls) or 12.5 μs/pixel (FITC and F-SWNTS diffusion into the cytopolasm). The scan area was 256 × 256 pixels and 100 frames were collected for each experiment. The digital zoom of the microscope was set to 16.4, which corresponds to a pixel size of 50 nm and a region of 12.5 μm^2. For the FITC excitation, we used the 488 nm line of the argon ion laser. The imaging parameters were adjusted as described in Rossow *et al*.[15] Data were collected in the pseudo photon counting mode of the Olympus FV 1000 microscope. We used the SimFCS program (Laboratory for Fluorescence Dynamics). Data were collected in the 256 × 256 frame format. Fitting of the RICS function was carried out according to the equations for diffusion as described in Digman *et al* after removal of the immobile fraction.[16-18] For each simulation or experiment, the RICS function is calculated as the average of all images of the stack. For the calculation of scan analysis, a small region of interest (64 × 64 pixels) was systematically moved across the image by steps of 32 pixels providing a partial superposition of the regions explored. This enabled to measure diffusion values at different subcellular locations (Figs. 3c,e).

Transmission electron microscopy: *C. roseus* cells were treated with 0.4 mg/mL F-SWNTs/probenecid for 3 h. The cells were then fixed with 4% glutaraldehyde in MSMO (Murashig and Skoog with minimal organics) for 1 h at room temperature and then kept in a refrigerator overnight. After rinsing with 0.05 M potassium phosphate buffer (pH 7.0), the cells were post-fixed in 2% osmium tetroxide for 1 h. They were then dehydrated through a graded series of acetone and embedded in Spurr's resin. Ultra-thin sections (approximately 90 nm thick) were cut with a diamond knife on an ultramicrotome (Leica ultracut S). After staining with uranyl acetate and lead citrate, sections were observed in a JEOL JEM 2100F TEM at an accelerating voltage of 200 kV. Images were taken on a Gatan 1k×1k CCD Camera.

a

Scan Speed (µs)	Laser Transmission	$G_{RICS}(0):R_f$ (approximate ratio)
8 µs	1%	--- (divergence of fit)
	2%	2:1
	2.5%	4:1
	3%	8:1
	3.5%	7:1
	4%	5:1
	4.5%	8:1
	5%	5:1

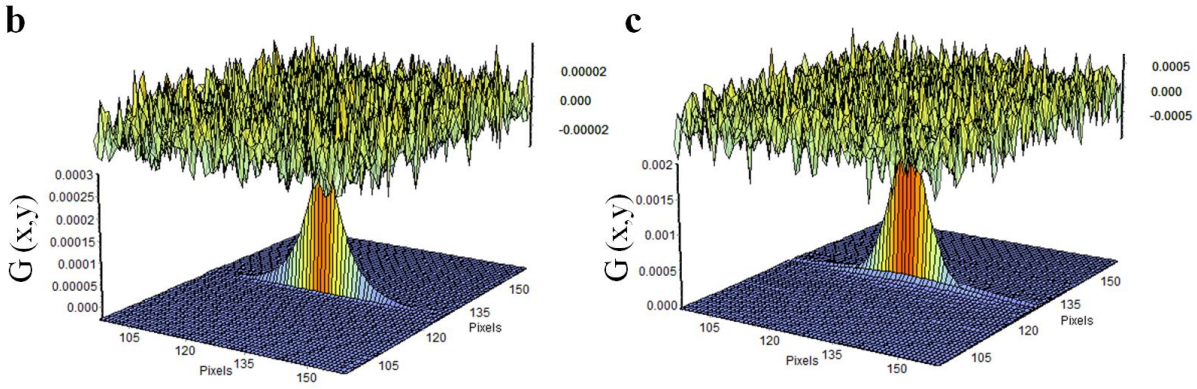

Figure 1. Typical laser beam waist calibration results for RICS measurements. a) The table illustrates the magnitude of the correlation fit at origin [$G_{RICS}(0)$] / the residuals-of-the-fit (R_f) ratios at a serial values of laser transmissions using a confocal scan speed of 8µs. b) The graph illustrates the fit of the autocorrelation function of FITC in PBS (D = 272 $\mu m^2 s^{-1}$ at 25°C). c) The graph illustrates the fit of the autocorrelation function of F-SWNTs (D = 92.78 $\mu m^2 s^{-1}$ at 25°C in PBS).

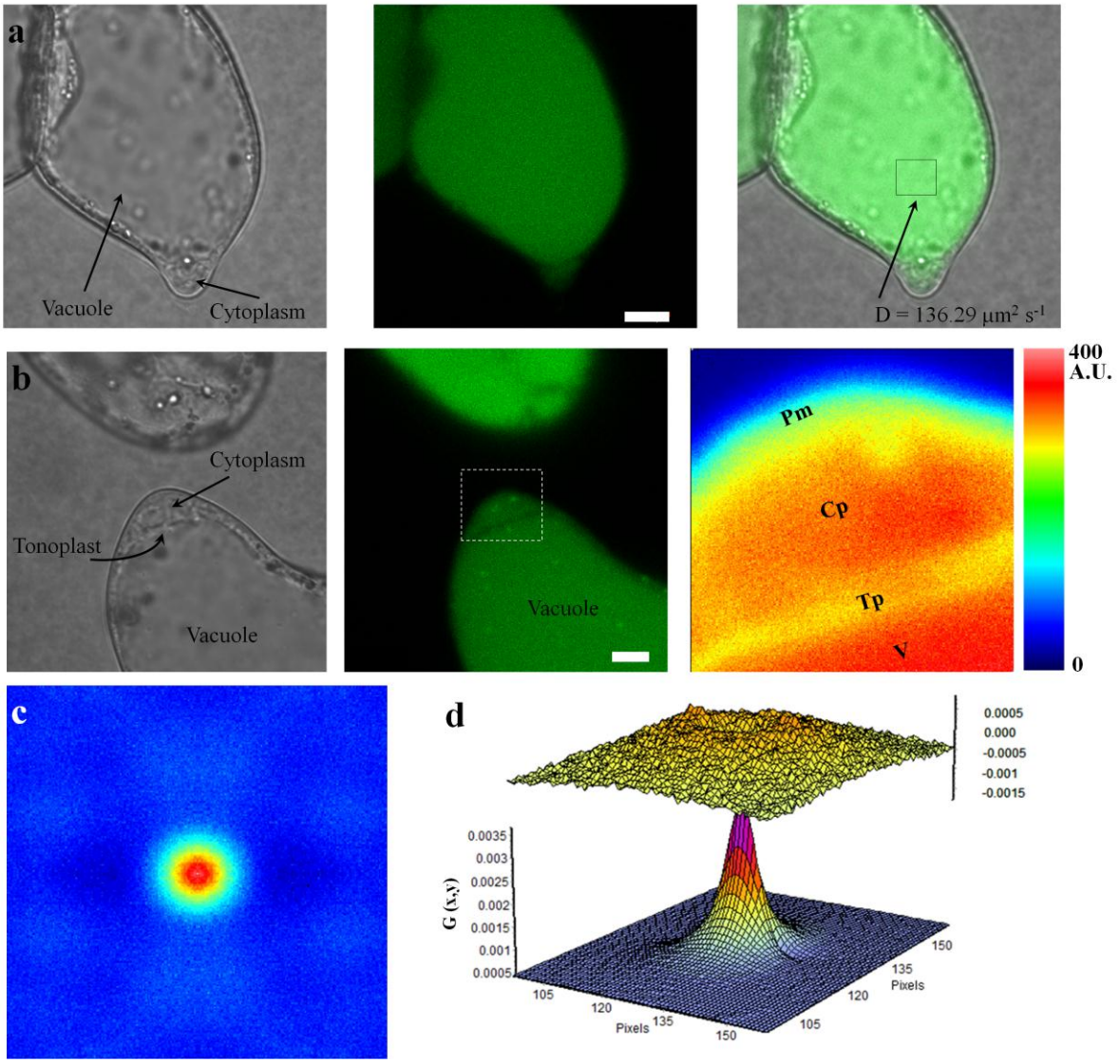

Figure 2. RICS analysis of FITC in *Catharanthus* cells. a) Confocal imaging of FITC distribution in *Catharanthus* cells prior to RICS analysis of FITC diffusion in the vacuole. The Left image is a bright-field image, while the right one is the merged image. The ROI marked with the square in the cell vacuole (right image) was zoomed and subjected to RICS analysis. RICS analysis resulted in a diffusion value of 136.29 $\mu m^2 s^{-1}$. Scale bar is 10 µm. b) Confocal imaging of FITC distribution in *Catharanthus* cells prior to RICS analysis of FITC diffusion into the cytoplasm. The ROI marked with the white square (middle image) was zoomed and subjected to RICS analysis. The intensity map (right image) illustrates the average intensity of 50 frames of

the ROI identified inside the square. Scale bar 5 μm. c) The spatial autocorrelation of the intensity data from the white square in Fig. 2b. d) The fit of the autocorrelation function for the ROI gives a diffusion value of 1.85 $\mu m^2 s^{-1}$. Pm: plasmalemma, Cp: cytoplasm, Tp: tonoplast, V: vacuole.

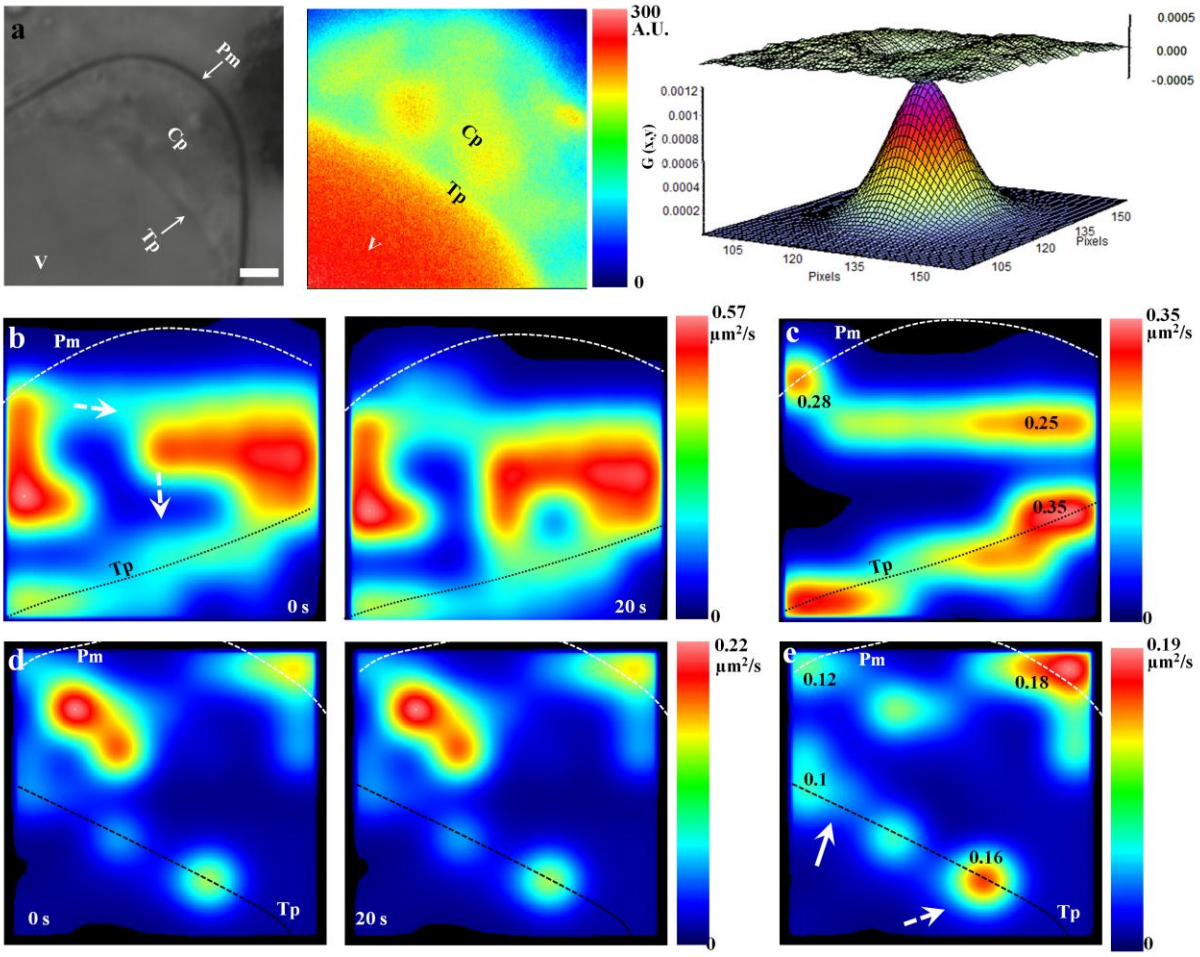

Figure 3. Spatial diffusion of FITC and F-SWNTs in the cytoplasm of *Catharanthus* cells. a) Bright field (left image) and average intensity mapping (middle image) of F-SWNTs accumulation in the vacuole and the cytoplasm of *Catharanthus* cell. The fit of the autocorrelation function (right image) for the region of the cell displayed in the intensity map (middle image) gives a diffusion value of 0.99 $\mu m^2 s^{-1}$. Scale bar: 10µm. Areas of the cytoplasm with no vacuolar structures were chosen for the RICS analysis because the presence of vacuolar structures often results in an increased diffusion values because of their intrinsic mobility. b) Spatial mapping of the subcellular dynamics of FITC (left image). Arrows indicate the direction of the diffusion trajectories appeared after 20 s (right image). The spatial maps were obtained by scanning a 32 × 32 pixel sequentially over the whole data shown in Fig. 2b,c. Outliers and fast

diffusion values of the cell vacuole were set to zero to resolve the cytoplasmic diffusion values (see Supplementary Text II). A mask of the plasmalemma (Pm) and the tonoplast (Tp) is overlaid as a topographical map. c) Faster diffusion values of the cytoplasm were set to zero to scale up the tonoplast diffusion values. Numbers indicate the local diffusion values at different cellular sub-locations. d) Spatial mapping of the subcellular dynamics of F-SWNTs (left image). The slow diffusion of F-SWNTs hindered the resolution of temporal subcellular dynamics after 20 s (right image). c) Faster diffusion values of the cytoplasm were set to 0 to scale up the tonoplast diffusion values. Numbers indicate the local diffusion values at different cellular sub-locations. The solid arrow indicates a zone of the tonoplast with continuous transport activity. The dashed arrow indicates a zone of localized transport activity. The spatial maps were obtained by scanning a 32 × 32 pixel sequentially over the whole data shown in (a). Pm: plasmalemma, Cp: cytoplasm, Tp: tonoplast, V: vacuole. Figures b–e are 12.8μm × 12.8μm.

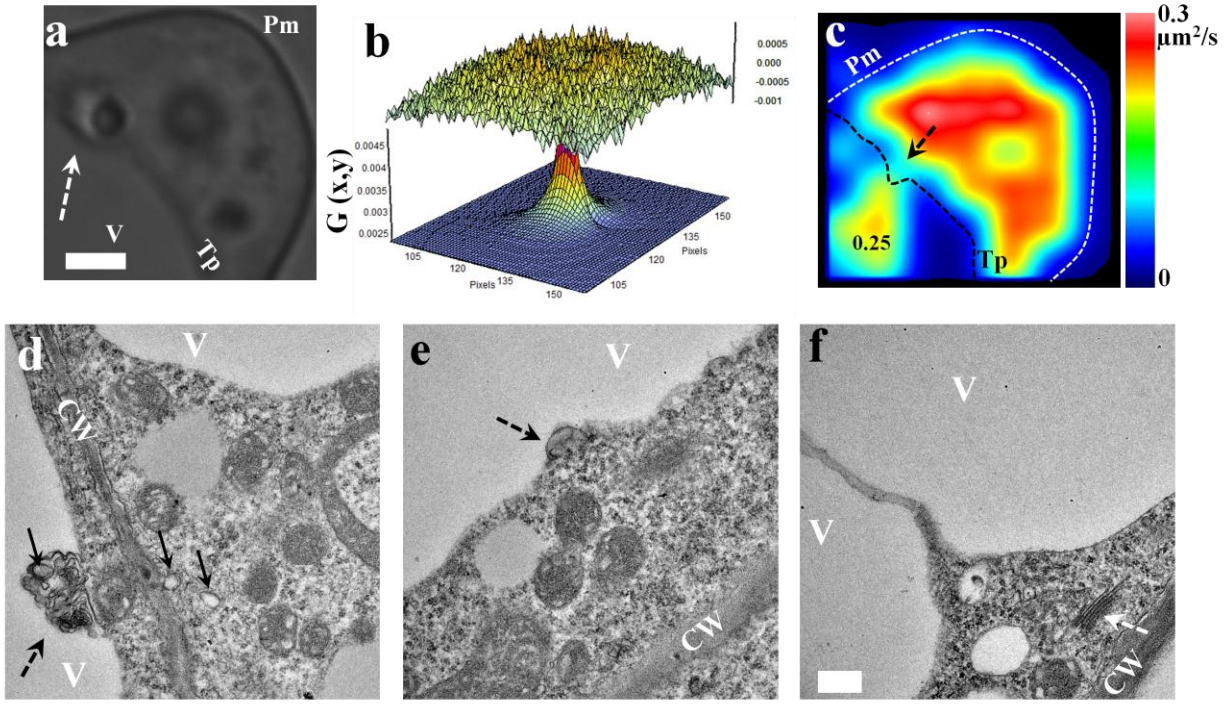

Figure 4. Autophagy-based transport of F-SWNTS revealed *via* HRTEM and RICS analysis. a) Bright filed imaging of a cell incubated with probenecid and F-SWNTs. The arrow indicates shedding of a damaged organelle into the cell vacuole. Scale bar is 5 µm. b) The graph shows the fit of the autocorrelation function for the region of the cell displayed in (a). This fit was used to construct the spatial map of F-SWNTs diffusion. c) Spatial mapping of the subcelluar dynamics of F-SWNTs in *Catharanthus* cells incubated in medium containing probenecid. The subcellular dynamics at the tonoplast were absent except at defined locations of autophagy (dashed arrow). The arrow indicates the zone showing autophagy with a localized transport activity. The relatively higher cytoplasmic diffusion of F-SWNTs is attributed to the presence of mobile vacuolar structures (a). Pm: plasmalemma. Tp: tonoplast. d) HRTEM micrograph illustrating the formation and transport of autophagosomes into cell vacuole. Dashed arrows indicate damaged Golgi bodies inside a cell vacuole. Solid arrows indicate smaller vesicular bodies possibly associated with Golgi apparatus. Cells were incubated with F-SWNTs for 3 h prior to TEM

imaging. e) Cytoplasmic and vacuolar view of cells incubated with F-SWNTs. The black dashed arrow indicates localized transport of a damaged organelle into a cell vacuole. f) Cytoplasmic and vacuolar view of cells incubated in F-SWNTs-free medium. No sign of autophagy was observed. The white arrow indicates an intact Golgi apparatus. CW: cell wall. V: vacuole. Scale bar is 350 nm.

Supporting Information. A brief introduction on RICS approach, documentation on the removal of outliers and fast diffusion values from the spatial maps and additional results including: RICS analysis of vacuolar and cytoplasmic accumulation of SWNTs and HRTEM imaging of the autophagy phenomenon. This material is available free of charge via the Internet at http://pubs.acs.org.

AUTHOR INFORMATION

Corresponding Author

* Chemical and Life Sciences and Engineering Division, King Abdullah University of Science and Technology, Thuwal 23955-6900, SAUDI ARABIA. E-mail: (magedserag@yahoo.com).

Notes

The fluorescence data were analyzed using the Globals software package developed at the Laboratory for Fluorescence Dynamics at the University of Illinois at Urbana-Champaign. The experimental work and data analysis were done in the Department of Applied Chemistry, Nagoya University, Japan.

ACKNOWLEDGMENT

This research was partly supported by the Industrial Technology Research Grant Program from the New Energy and Industrial Technology Development Organization (NEDO) of Japan and the Japan Society for the Promotion of Science (JSPS) through its “Funding Program for World-Leading Innovative R&D on Science and Technology (FIRST Program)”. M. F. S. wishes to extend a sincere gratitude to Prof. Jason R. Dwyer at University of Rhode Island (USA) for his valuable contributions during writing the manuscript. AB wishes to thank CNRS and JSPS for the invited fellowship in the framework of the Invitation Fellowship Program for Research in

Japan (ID No. S-12072). The authors wish to thank Prof. Marcel Ameloot and Dr Ben De Clercq at Hasselt University (Belgium) and Dr Frédéric Gros at University of Strasbourg (France) for helpful discussions and comments.

REFERENCES

[1] Kostarelos, K.; Lacerda, L.; Pastorin, G.; Wu, W.; Wieckowski, S.; Luangsivilay, J; Godefroy, S.; Pantarotto, D.; Briand, J.; Muller, S.; Prato, M.; Bianco, A. *Nature Nanotechol.* **2007**, *2*, 108.

[2] Liu, Z.; Sun, X.; Nakayama-Ratchford, N.; Dai, H. *ACS Nano.* **2007**, *1*, 50.

[3] Liu, Z.; Cai, W.; He, L.; Nakayama, N.; Chen, K.; Sun, X.; Chen, X.; Dai, H. *Nature Nanotechol.* **2007**, *2*, 47.

[4] Kagan, V. E.; Konduru, N. V.; Feng, W.; Allen, B. L.; Conroy, J.; Volkov, Y.; Vlasova, I. I.; Belikova, N. A.; Yanamala, N.; Kapralov, A.; Tyurina, Y. Y.; Shi, J.; Kisin, E. R.; Murray, A. R.; Franks, J.; Stolz, D.; Gou, P.; Klein-Seetharaman, J.; Fadeel, B.; Star, A.; Shvedova, A. A. *Nature Nanotechol.* **2010**, *5*, 354.

[5] Al-Jamal, K. T.; Nunes, A.; Methven, L.; Ali-Boucetta, H.; Li, S.; Toma, F. M.; Herrero, M. A.; Al-Jamal, W. T.; Ten Eikelder, H. M.; Foster, J.; Mather, S.; Prato, M.; Bianco, A.; Kostarelos. K. *Angew. Chem. Int Ed Engl.* **2012**, DOI: 10.1002/anie.201201991.

[6] Serag, M. F.; Kaji, N.; Tokeshi, M.; Baba Y. *RSC. Adv.* **2012**, *2*, 398.

[7] Shvedova, A. A.; Kisin,E. R.; Porter,D.; Schulte, P.; Kagan, V. E.; Fadeel, B.; Castranova. V. *Pharmacol. Ther.* **2009**, *121*, 192.

[8] Serag, M. F.; Kaji, N.; Tokeshi, M.; Bianco, A.; Baba, Y. *Integr. Biol.* **2012**, *4*, 127.

[9] Yang, W.; Thordarson, P.; Gooding, J.; Ringer, S. P.; Braet. F. *Nanotechnology.* **2007**, *18*, 1.

[10] Serag, M. F.; Kaji, N.; Venturelli, E.; Okamoto, Y.; Terasaka, K.; Tokeshi, M.; Mizukami, H.; Braeckmans, K.; Bianco, A.; Baba, Y. *ACS Nano.* **2011**, *5*, 9264.

[11] Serag, M. F.; Kaji, N.; Gaillard, C.; Okamoto, Y.; Terasaka, K.; Jabasini, M.; Tokeshi, M.; Mizukami, H.; Bianco, A.; Baba,Y. *ACS Nano.* **2011**, *1*, 493.

[12] Liu, Q.; Chen, B.; Wang, Q.; Shi, X.; Xiao, Z.; Lin, J.; Fang, X. *Nano Lett.* **2009**, *9*, 1007.

[13] Kim, S. A.; Heinze, K. G.; Schwille, P. *Nat. Methods.* **2007**, *4*, 963.

[14] Vámosi, G.; Damjanovich, S.; Szöllősi, J.; Vereb, G. *Curr. Protoc. Cytom.* **2009**, *2*, 2.15.

[15] Rossow, M. J.; Sasaki, J. M.; Digman, M. A.; Gratton, E. *Nature Prot*. **2010**, *5*, 1761.

[16] Digman, M. A.; Gratton, E. *Microsc. Res. Tech*. **2009**, *72*, 323.

[17] Digman, M. A.; Wiseman, P. W.; Horwitz, A. R.; Gratton, E. *Biophys. J.* **2009**, *96*, 707.

[18] Digman, M. A.; Brown, C. M.; Horwitz, A. R.; Mantulin, W. W.; Gratton, E. *Biophys. J.* **2008**, *94*, 2819.

[19] Petrášek, Z.; Schwille, P. *Biophys. J.* **2008**, *94*, 1437.

[20] Widengren, J.; Mets, Ü.; Rigler, R. *J. Phys. Chem.* **1995**, *99*, 13368.

[21] Periasamy, N.; Verkman A. S. *Biophys. J.* **1998**, *75*, 557.

[22] Makhzoum, A.; Petit-Paly, G.; St Pierre, B.; Bernards, M. A. *Plant Cell Rep.* **2011**, *30*, 1173.

[23] Brinkley, M. *Bioconjug. Chem.* **1992**, **3,** 2.

[24] Minibayeva, F.; Dmitrieva, S.; Ponomareva, A.; Ryabovol, V. *Plant Physiol. Biochem*. **2012**, DOI: 10.1016/j.plaphy.2012.02.013.

[25] Chen, S.; Rehman, S. K.; Zhang, W.; Wen, A.; Yao, L.; Zhang, J. *Biochim Biophys. Acta* **2010,** *1806*, 220.

The table of contents entry